Applied Clay Science 235 (2023) 106866

Contents lists available at ScienceDirect

Applied Clay Science

journal homepage: www.elsevier.com/locate/clay

Research Paper

The adsorption behavior of niobium (V) on kaolin clay and kaolinite

Tingting Yang [a,b], Ning Wang [a], Hannian Gu [a,b,*]

[a] Key Laboratory of High-temperature and High-pressure Study of the Earth's Interior, Institute of Geochemistry, Chinese Academy of Sciences, Guiyang 550081, China
[b] University of Chinese Academy of Sciences, Beijing 100049, China

ARTICLE INFO

Keywords:
Niobium
Adsorption behavior
Kaolin clay
Kaolinite

ABSTRACT

Niobium (Nb) in kaolin clay usually occurs in the Ti-bearing minerals, such as rutile and anatase. However, the low Ti-bearing minerals contents for some kaolin clay rocks were insufficient to explain the high Nb concentrations. Thus, Nb was widely considered to be adsorbed by clay minerals. However, the adsorption behavior of niobium (V) on clay minerals has not been fully understood. In this study, a series of batch adsorption experiments were carried out on kaolin clay (Kclay) and pure kaolinite (Kaol) using niobium oxalate solutions. The effects of contact time, initial niobium (V) concentration, solution pH, and temperature on the adsorption were investigated. The results showed that Kclay exhibited a higher adsorption capacity than Kaol under the same conditions. The niobium (V) adsorptions on Kclay and Kaol were pH-dependent, and both of them showed declining adsorption capacities from pH 2 to 4. The adsorption behaviors of niobium (V) on Kclay and Kaol conformed to the pseudo-second-order model. The adsorption isotherm of Kclay was a better fit with the Freundlich isotherm model, while the Langmuir isotherm model was a better fit for Kaol. The Langmuir maximum adsorption amount of Kclay and Kaol were 5.42 and 2.25 mg/g, respectively. These results demonstrated that niobium (V) can be adsorbed by kaolin clay and kaolinite.

1. Introduction

Niobium (Nb), as a critical strategic resource, has been extensively applied in aerospace, steel, superconducting magnets, national defense, nuclear industry, and electronic manufacturing (Schlewitz, 2009; USGS, 2022; Sun et al., 2022). The world's highest niobium mine reserve was in Brazil with 16 million tons, followed by Canada with 1.6 million tons, accounting for >98% of the global niobium mine reserves (Zhu et al., 2021; USGS, 2022). The unbalanced distribution of Nb resources has been considered to result in supply security being at risk for other countries (Mackay and Simandl, 2014). For example, Nb was not mined in either China or the United States, leading to their high import-reliance because the consumptions exceed their domestic resources or processing capacity (Gulley et al., 2018). Thus, to develop diversified new Nb resources can reduce the supply risk for niobium-deficient countries.

Nb-containing clay rocks from the bottom of the Xuanwei Formation of the Late Permian sequences were discovered as potential Nb resources in eastern Yunnan, western Guizhou, and southern Sichuan of China (Dai et al., 2010; Zhao et al., 2016a, 2016b, 2017). The major minerals in the clay rocks were kaolinite, anatase, iron-bearing minerals, and Ti-bearing minerals (Zhang et al., 2016; Wang et al., 2018). Notably, the Nb concentration of the kaolin clay rocks was reported to be in the range of 200–600 μg/g (Wang et al., 2018), which reached the minimum industrial grade requirement (Nb_2O_5 160 to 200 μg/g) for weathering crust-type Nb deposits in China (MNR, 2020). The Nb-containing clay had the characteristics of a wide distribution area and large resources with a significant resource potential for exploitation (Zhang et al., 2016; Zhu et al., 2021). The kind of clay type Nb resource has not been effectively exploited due to inadequate recognition of the occurrence state of Nb. Previously, it was reported that Nb occurred in Ti-bearing minerals, such as ilmenite, rutile, anatase, etc. (Schlewitz, 2009; Mackay and Simandl, 2014; Gibson et al., 2015). Indeed, Nb-ilmenite and anatase as dispersed fine particles have been identified in the above clay samples (Zhao et al., 2017; Zhu et al., 2021). However, the low Nb-ilmenite and anatase contents were insufficient to interpret the high Nb contents in bulk clay samples (Zhao et al., 2017). Therefore, Dai et al. (2010) and Zhao et al. (2017) proposed that Nb might be adsorbed in clay minerals.

Several studies have been reported on the adsorption of Nb on clay minerals and soils. For instance, the adsorption of niobium on kaolinite (soil constituent minerals) was pH-dependent with a high distribution coefficient of 100–500 m^3/kg (Ervanne et al., 2014; Söderlund et al.,

* Corresponding author at: NO.99 Lincheng West Road, Guanshanhu District, Guiyang City, Guizhou Province 550081, China.
E-mail address: guhannian@vip.gyig.ac.cn (H. Gu).

https://doi.org/10.1016/j.clay.2023.106866
Received 11 August 2022; Received in revised form 4 February 2023; Accepted 11 February 2023
Available online 21 February 2023

2015; Yamaguchi et al., 2020). Niobium adsorption on kaolinite and illite could occur as several different surface species (Ervanne et al., 2014; Yamaguchi et al., 2020). Nonetheless, except for the effect of pH and contact time, these studies did not provide in-depth research on the effects of other adsorption conditions such as initial niobium (V) concentration and solution temperature on niobium (V) adsorption by clay minerals. The deficiency of understanding niobium (V) adsorption on clay minerals motivated us to conduct batch adsorption experiments to investigate niobium (V) adsorption behavior on kaolin clay and kaolinite. In this work, the effects of contact time, initial niobium (V) concentration, solution pH, and solution temperature on the niobium (V) adsorption behavior of kaolin clay and kaolinite were investigated. The adsorption kinetics and isotherms were fitted using different models to describe the adsorption process. The insights of this study would be useful to clarify the occurrence state of Nb in Nb-rich kaolin clay rocks.

2. Materials and methods

2.1. Materials and chemicals

The kaolin clay (labeled as Kclay) for the experiments was collected from Weining, Guizhou Province, China. Kclay samples were crushed, ground, and sieved. The kaolinite purchased from Sigma-Aldrich was a relatively pure mineral (labeled as Kaol). Kclay and Kaol samples were ground to pass 200-mesh sieve (74 μm) to minimize the influence of different particle sizes for the subsequent experiment. They were then dried in a drying oven at 85 °C for 24 h before being cooled to room temperature and stored in sealed plastic bags in a desiccator for experiments. Niobium oxalate (98%, $Nb(HC_2O_4)_5$) as the source of niobium (V) was purchased from Shanghai Yien Chemical Technology Co., Ltd. of China. Other chemicals used in the experiments were oxalic acid dihydrate (≥99.5%, $H_2C_2O_4{\cdot}2H_2O$) and ammonia solution (AR Grade), which were purchased from Tianjin Yongda Chemical Reagent Co., Ltd. and Tianjin Kemiou Chemical Reagent Co., Ltd., respectively. All chemicals in the studies were used as received, without further purification, and all solutions were prepared with deionized water (conductivity, 1.43 μS/cm).

2.2. Analysis and characterization methods

The chemical compositions of the samples were determined by X-ray fluorescence (XRF, PANalytical PW2424, Netherlands) spectroscopy. A prepared sample was fused with a lithium metaborate–lithium tetraborate flux which also included an oxidizing agent (lithium nitrate) and was then poured into a platinum mold. After that, the obtained disk was analyzed by XRF spectrometry. The XRF analysis was examined in conjunction with a loss-on-ignition (LOI) at 1000 °C, and the resulting data came from the combination of the two methods. The trace element analysis of the Kclay and Kaol was determined by inductively coupled plasma mass spectrometry (ICP-MS). The digestion process was performed as follows (Sjöqvist et al., 2013; Gu et al., 2018): Each sample (0.2 g) was decomposed with 0.9 g lithium metaborate/lithium tetraborate with intensive mixing, and fused at 1025 °C. The fused sample was then cooled and dissolved in a 100 mL solution of 4% HNO_3 and 2% HCl. Finally, the solution was analyzed by ICP-MS (Perkin Elmer Elan 9000, USA). The niobium concentrations in solutions before or after adsorption were directly measured by ICP-MS (Perkin Elmer NexION 300×, USA) without digestion treatment.

The X-ray diffraction (XRD) patterns of the samples were recorded using a powder X-ray diffractometer (PANalytical Empyrean, Netherlands) utilizing Cu *Kα* radiation. The apparatus was conducted under standard conditions at 40 kV, 20 mA. The XRD spectra were scanned at a 2θ range from 5° to 60° at a speed of 10°/min, with a step length of 0.03°. The transmission electron microscopy (TEM) images of samples were observed by a Tecnai G2 F20 S-Twin (FEI Company, USA) field emission transmission electron microscope with energy dispersive spectroscopy (EDS). The EDS was worked with an accelerating voltage of 20 kV and beam current of 1 nA. Approximately 1 g sample was dispersed into ethyl alcohol suspension for 5 min using an ultrasonic disperser, and a droplet of the sample dispersion was then dropped onto a lacy carbon-coated 20-mesh Cu grid and transferred to the microscope for observation after drying.

Particle size distribution and specific surface area of Kclay and Kaol were characterized by an LS 13320 laser particle size analyzer (Beckman Coulter Inc., USA) and a nitrogen adsorption apparatus (Autosorb-iQ2-MP, Quantachrome, USA), respectively. The measuring range of the laser particle size analyzer was 0.04–2000 μm. Each sample (1 g) to be tested was dispersed into ethyl alcohol via ultrasonication for 10 min before particle size determination. For the determination of specific surface area, samples were vacuum-degassed at 150 °C for 12 h, and the results were obtained at −196 °C from relative pressure (P/P_0) 0.05–0.20. The specific surface areas were calculated by the multi-point BET (Brunauer-Emmett-Teller) method (Brunauer et al., 1938). The point of zero charge (pH_{PZC}) of Kclay and Kaol were conducted using an automatic potentiometric titrator (T50, Mettler Toledo, Switzerland) with a glass electrode (DGi111-SC, Mettler Toledo). A suspension was prepared by placing a 1.5 g sample in 150 mL of deionized water and was shaken at 25 °C for 2 days. The titration was carried out by placing the above suspension into a 200 mL titration cup at 25 °C. Initially, the suspension pH was quickly lowered to approximately 2.6 by 0.5 mL HCl (3 mol/L). The suspension was then slowly titrated up to pH 11 with 2 mol/L NaOH. A similar titration was performed on the supernatant obtained by centrifugation of the suspension (Yu et al., 2020).

2.3. Batch adsorption experiments

Considering that Kclay contained 514 μg/g of Nb, the Nb-releasing process was investigated and the results (Table S1, seen in Supplementary Material online) showed that the releasing amounts of Nb from Kclay were negligible. The adsorption of niobium (V) on the Kclay and Kaol sample was investigated in $Nb(HC_2O_4)_5$ aqueous solutions in a batch system. All batch adsorption experiments were conducted in a conical flask placed on a thermostatic shaker (THZ-82A, Changzhou, China). For each experiment, the sample (2.000 g) and niobium (V) solution (200 mL) were mixed in the conical flask (solid/liquid ratio of 10 g/L), which was then shaken in the thermostatic shaker (200 rpm) for 300 min. A series of parameters including contact time (5–300 min), initial niobium (V) concentration (0.01–2.00 mmol/L), initial pH (1, 2, 3.3, 4, and 5), and temperatures (25-50 °C) on the influence of adsorption niobium (V) by Kclay and Kaol were systematically explored. The maximum niobium (V) concentration used was constrained by the low solubility of niobium oxalate. The initial pH was adjusted by 1 mol/L oxalic acid or ammonia solution. The pH of the solution was not adjusted except to investigate the influence of initial pH on adsorption. Subsequently, the dispersions were centrifuged at 3000 rpm for 3 min, and the solid clay minerals were separated from the supernatant solutions. The solid clay minerals were dried at 65 °C for 24 h and stored in sealed bags at 25 °C for further analysis. The supernatant solutions were subsequently filtered through 0.45 μm cellulose nitrate membranes for ICP-MS determination. The solution pH was measured at the beginning and end of each experiment. Each adsorption experiment group was conducted in triplicate to effectively reduce the experimental error. All data presented were the mean values of three replicate experiments.

The amount of the adsorbed niobium (V) per unit mass of the adsorbent (q_t, mg/g) was calculated followed by Eq. (1) (Albadarin et al., 2017).

$$q_t = \frac{(C_0 - C_t)VM}{m} \quad (1)$$

where C_o and C_t (mmol/L) refer to the initial niobium (V) concentration and the niobium (V) concentration in the solution at time t, respectively,

V (L) is the volume of oxalate niobium solution, M (g/mol) is the molar mass of niobium (V), and m (g) is the mass of adsorbent.

2.4. Adsorption kinetics and isotherms

The pseudo-first-order and pseudo-second-order models were undertaken to explore the factors that influence the adsorption rates of adsorbent and understand the dynamics of the adsorption process (Lagergren, 1898; Ho and McKay, 1999), as shown in Eqs. (2) and (3):

$$\text{Pseudo}-\text{first}-\text{order equation } q_t = q_e\left(1-e^{-k_1 t}\right) \quad (2)$$

$$\text{Pseudo}-\text{second}-\text{order equation } q_t = \frac{q_e^{\,2} k_2 t}{1+k_2 q_e t} \quad (3)$$

where q_e (mg/g) is the amount of the adsorbed Nb per unit mass of adsorbent at equilibrium, and k_1 (1/min) and k_2 (g·mg^{-1}·min^{-1}) are the rate constant of pseudo-first-order and pseudo-second-order, respectively.

Langmuir and Freundlich isotherms were applied to describe the adsorption behavior, which can be expressed as Eqs. (4) and (5) (Langmuir, 1916; Freundlich, 1906):

$$\text{Langmuir equation } q_e = \frac{q_{max} K_L C_e}{1+K_L C_e} \quad (4)$$

$$\text{Freundlich equation } q_e = K_F C_e^{\,1/n} \quad (5)$$

where C_e (mmol/L) is the adsorbate concentration at equilibrium in the aqueous solution, q_{max} (mg/g) is the maximum adsorption amount, K_L (L/mmol) is the Langmuir equilibrium constant which is related to the free energy of the adsorption, K_F ((mg/g)·(L/mmol)$^{1/n}$) is the Freundlich adsorption constant that related to adsorption capacity, and n is dimensionless unit correlates with characterizing surface heterogeneity.

3. Results and discussion

3.1. Characterization of samples

The chemical compositions and trace elements of Kclay and Kaol samples are presented in Table 1 and Table 2, respectively. From the results, the Al_2O_3 and SiO_2 values of Kaol were closer to ideal stoichiometric kaolinite (39.50% Al_2O_3 and 46.54% SiO_2, 13.96% LOI) (Awad et al., 2017), while Al_2O_3 and SiO_2 values in Kclay were lower due to their high impurities. TiO_2 and Fe_2O_3 were the common impurities in kaolin clay (Schroeder et al., 2003), and the results indicated that Kclay used was kaolin clay rock and Kaol used can be considered pure kaolinite mineral. Other minor component oxides discovered in Kclay and Kaol samples were P_2O_5, MgO, K_2O, etc. The Nb concentration of Kclay (514 μg/g) was obviously higher than that in Kaol (Table 2). Meanwhile, compared to Kaol, the Kclay sample used in this study contained higher trace impurities such as zirconium and lanthanides. Fig. 1a depicts the prominent characteristic diffraction reflections of XRD patterns for Kclay and Kaol utilized in batch experiments. The major mineral in Kclay, according to the XRD pattern, was kaolinite, with minor minerals of anatase and rutile, while the Kaol was entirely composed of kaolinite (Fig. 1a). The XRD results of Kclay and Kaol were compatible with XRF results (Table 1). The particle size distribution of Kclay and Kaol is shown in Fig. 1b, and the average particle sizes D50 in Kclay and Kaol were 0.60 μm and 7.14 μm, respectively. The particle size distribution results of Kclay and Kaol were in accordance with specific surface area analyses, from which Kclay and Kaol were 47.3 and 12.5 m^2/g. These results indicated that the clay aggregates were dissociated and dispersed well.

3.2. The effect of contact time and initial niobium (V) concentration

The adsorption of niobium (V) on Kclay and Kaol was investigated as a function of contact time to establish the equilibrium time of adsorption using 0.1 mmol/L Nb solution (Fig. 2a). The condition was controlled at a solid/liquid ratio (S/L) of 10 g/L, reaction temperature of 25 °C, and natural pH of 3.8. The rapid initial adsorption of niobium (V) on Kclay and Kaol took place at the early stage of initial time (5–10 min), followed by a much slower adsorption rate, and finally reached equilibrium within 30 and 120 min, respectively. As discussed, Kclay had a larger specific surface area than Kaol, so it could be expected that Kaol would take a longer time to reach the adsorption equilibrium. The fast adsorption process could be attributed to the easily accessible active sites on the bare surface of samples in the initial stages, but as the sites were covered by the adsorbate, the rate slowed in later stages (Abidi et al., 2017; Zhu et al., 2018). From the resluts, the adsorption amount at equilibrium for Kclay and Kaol were 0.97 and 0.56 mg/g, respectively. A contact time of 300 min was used for all the following experiments to ensure reaching the adsorption equilibrium.

The equilibrium adsorption capacities as functions of the different initial niobium (V) concentrations (0.01, 0.05, 0.1, 0.5, 1, and 2 mmol/L) on Kclay and Kaol were investigated under the condition of 25 °C, natural pH, and 300 min (Fig. 2b). The results showed that the adsorption capacities for Kclay and Kaol increased with the initial niobium (V) concentration increased until the equilibrium state. The results also suggested that the increase in the initial niobium (V) concentrations provided the mass transfer driving force of the niobium (V) between the aqueous solution and adsorbent phase, leading to an increase in niobium (V) adsorption amounts (Dönmez and Aksu, 2002; Alshameri et al., 2018). As Sei et al. (2002) reported, iron oxides could contribute to the large phosphate (oxyanions) adsorption amount of natural kaolinite samples. Similarly, the fact that Kclay had higher niobium (V) adsorption amounts than Kaol could be attributed to the impurities of Fe- and Ti- mineral phases in Kclay having a strong affinity for niobium (Ghosh et al., 2017). Additionally, the smaller particle sizes of Kclay were probably another factor contributing to its higher adsorption capacity. Although natural Nb concentrations in the geological process might be lower than the ones used, the adsorption experiments using high niobium concentrations in this study were to demonstrate the adsorption capacities of the clay samples.

3.3. The effect of solution pH and temperature

The surface charge and functional groups on the surface of Kclay and Kaol can be controlled by changing the pH of the solution. The behavior of niobium (V) adsorption on Kclay and Kaol at various solution pH values is depicted in Fig. 3a. The niobium (V) adsorption amounts of Kclay and Kaol showed a clear trend with the change of pH of the solution system. The niobium (V) adsorption amounts of Kclay and Kaol increased when pH was changed from 1 to 2, and then they decreased with a further increase in pH from 2 to 4. As the pH increased from 4 to 5, the niobium (V) adsorption amounts of both samples increased slightly. The adsorption behavior of niobium (V) at various pH values could be explained by the species of niobium (V) in solution as well as

Table 1
Chemical compositions of Kclay and Kaol (mass %).

Components	Al_2O_3	SiO_2	TiO_2	TFe_2O_3	P_2O_5	MgO	K_2O	CaO	Na_2O	LOI
Kclay	30.93	36.85	11.00	6.04	0.27	0.15	0.11	0.07	0.06	12.96
Kaol	36.66	47.34	0.34	0.46	0.45	0.13	1.51	0.08	0.05	12.51

Table 2
Trace element concentrations of Kclay and Kaol samples (μg/g).

Elements	Nb	Ta	V	Zr	Th	U	Ga	Hf	La-Lu
Kclay	514.0	31.0	658.0	3540.0	105.0	19.9	111.5	89.8	1381.2
Kaol	9.4	0.8	47.0	39.0	58.2	14.9	42.5	1.2	645.9

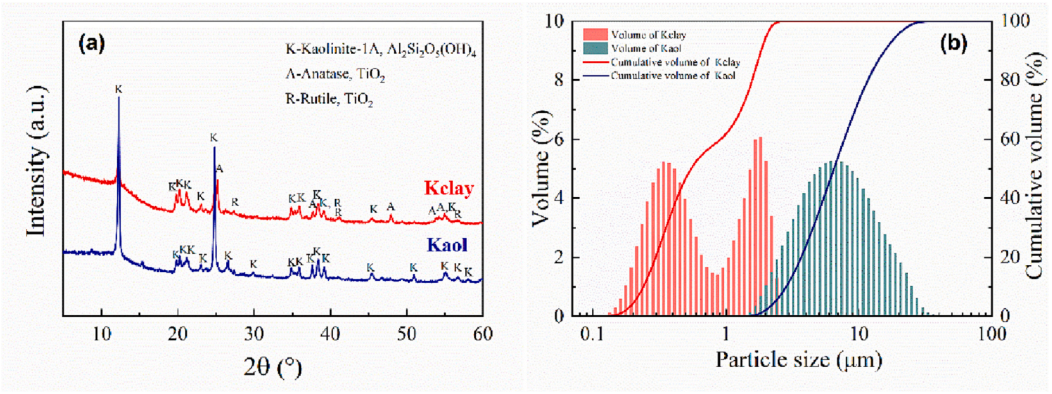

Fig. 1. (a) XRD patterns and (b) particle size distribution of Kclay and Kaol.

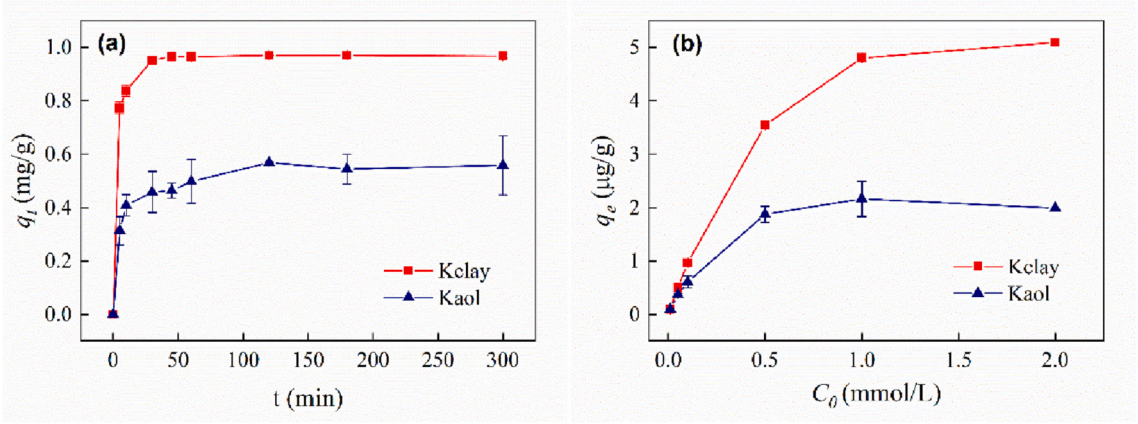

Fig. 2. The effect of (a) contact time and (b) initial niobium (V) concentration on the niobium (V) adsorption of Kclay and Kaol (S/L = 10 g/L, T = 25 °C).

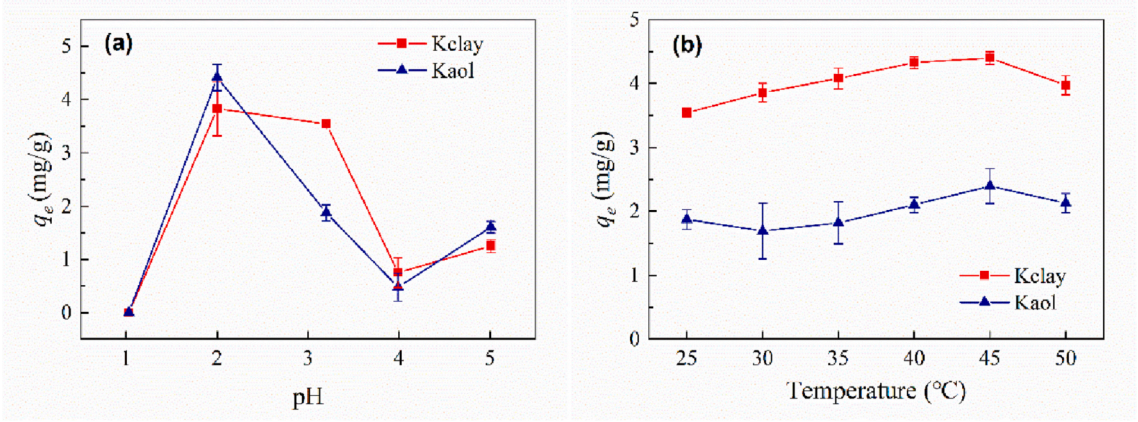

Fig. 3. The effect of (a) solution pH and (b) temperature on the niobium (V) adsorption by Kclay and Kaol (S/L = 10 g/L, C_0 = 0.5 mmol/L, t = 300 min).

pH_{PZC} of Kclay and Kaol.

The +V valence state is the most stable oxidation state of niobium (Söderlund et al., 2015; Ghosh et al., 2017). Niobium is poorly soluble in water and usually forms complex ions in solution (Charles and Prime, 1983; Lehto and Hou, 2010). While oxalic acid, as a strong complexing agent for Nb, would tend to form anionic complexes in solution (Steinberg, 1961; Charles and Prime, 1983). When the pH was <3, the dominant species of niobium (V) ions in the solution were [NbO

$(C_2O_4)_3]^{3-}$ and $[NbO(C_2O_4)_2(H_2O)]^-$. When pH ranged 3–4, the species of niobium (V) ions hydrolyzed into $[NbO(C_2O_4)_2(OH)_2]^{3-}$, $[NbOC_2O_4(OH_2)H_2O]^-$, and $[Nb_2O_4(C_2O_4)_2(H_2O)_2]^{2-}$ followed by decomposition into hydrous niobium oxide, $Nb_2O_5{\cdot}nH_2O$ (s). When pH was higher than 4, reactions happened including the decomposition of the niobium (V) species and the formation of a white and amorphous Nb hydrous oxide (Jehng and Wachs, 1991; Deblonde et al., 2019).

There were two types of charge existing on the surface of kaolinite. One was the permanent negative charge resulting from minor isomorphic substitution in the tetrahedral sheet, and the other was variable pH-dependent charge at the edges and the octahedral faces caused by the protonation or deprotonation of hydroxyls on the amphoteric sites, either positive or negative (Tombácz and Szekeres, 2006; Hu and Yang, 2013; Awad et al., 2017). The critical point of mineral surface protonation can be judged by the pH_{PZC}. The analysis results (Fig. S1, seen in Supplementary Material online) showed that the pH_{PZC} values of Kclay and Kaol were relatively close to 2.8 and 2.7, respectively, which were in the reported pH_{PZC} range (2.7–3.2) of kaolinite in the literature (Appel et al., 2003). When the pH value was lower than pH_{PZC} of Kclay and Kaol, the protonation of aluminol groups of kaolinite would take place as shown in Eq. (6) accompanying the formation of positive charges on broken edges. Within the range of pH lower than 3, the dominant species of niobium (V) in solution were the complex anions $[NbO(C_2O_4)_3]^{3-}$ and $[NbO(C_2O_4)_2(H_2O)]^-$ (Jehng and Wachs, 1991; Deblonde et al., 2019). The opposite charge between Kclay or Kaol and the complex anions niobium (V) would induce electrostatic attraction. In general, with pH declined, the protonation of aluminol groups would be stronger resulting in generating more positive charges on the surface of the kaolinite. Thus, the adsorption amount was enhanced when pH decreased from 3.3 (natrual pH of 0.5 mmol/L Nb solution) to 2 as a result of electrostatic interaction between the samples and niobium (V). At the pH of 1, the decrease in the amount of niobium (V) adsorption was due to the dissolution of Al and Si in kaolinite under such acid conditions (Khawmee et al., 2013). When the pH value was greater than pH_{PZC} of Kclay (2.8) and Kaol (2.7), the deprotonation of kaolinite by Eq. (7) resulted in the formation of negative charges. At pH higher than 3, the oxalate complexes of niobium (V) started to decompose into hydrous niobium oxide ($Nb_2O_5{\cdot}nH_2O$(s)). The decrease in adsorption amount at pH 3.3–4 could be attributed to the reduction of Kclay and Kaol positive charge capacity and adsorbable anion niobium (V) amount. Above pH of 4, the formation of a white and amorphous Nb hydrous oxide might directly decrease the concentration of niobium (V) in the solution, resulting in a slight increase in adsorption amount. The positive or negative charge formation of kaolinite surface was described following Eqs. (6) and (7) (Hu and Yang, 2013; Alshameri et al., 2019):

$$\equiv SOH + H^+ \rightarrow \equiv SOH_2^+ \quad (6)$$

$$\equiv SOH + H^- \rightarrow \equiv SO^- + H_2O \quad (7)$$

where ≡SOH represents adsorption sites at the kaolinite surface, and S stands for Al or Si.

The variable charges of clay minerals associated with pH changes were also involved in surface complexation reactions (Yu et al., 2020). The adsorption curves of Kclay and Kaol with pH changing as shown in Fig. 3a were similar to previous reports on niobium (V) adsorption behavior on ferric oxide colloid, pyrolusite, and silica colloid at different pH values (Ghosh et al., 2017, 2019, 2020). According to the adsorption mechanisms outlined in the above studies, Nb possessed both electrostatic adsorption and surface complexation adsorption. Ervanne et al. (2014) also hypothesized that niobium was adsorbed on the kaolinite surface by forming an inner-sphere complex through the formation of a chemical connection with the oxygen of the hydroxyl groups. Since the oxalate complexes of niobium (V) in this work and Nb in Ervanne et al. (2014) primarily occurred in solution as anions, it can be considered that the niobium (V) adsorption process in this study involved in surface complexation adsorption. In addition to electrostatic adsorption, the higher adsorption capacities in pH of 2 could also be explained by surface complexation between the surface hydroxyl group of kaolinite and the anions group of the Nb in acidic oxalate. The surface complexation was expected to be one of the adsorption mechanisms in this study, and the detailed confirmation of oxalate complexes of niobium (V) with Kclay and Kaol need be studied in future work.

Temperature was a vital parameter in adsorption study because it can affect the process in different ways including influencing the kinetics (Ghosh et al., 2020). The effect of temperature on niobium (V) adsorption on Kclay and Kaol was carried out at temperatures of 25 to 50 °C (Fig. 3b). The influences of temperature on the two samples showed similar trends. Kclay and Kaol adsorption capacities improved when temperature increased from 25 to 45 °C, with adsorption capacities ranging from 3.54 to 4.40 mg/g and 1.87 to 2.39 mg/g, respectively. The increasing temperature might contribute to better diffusion of niobium (V) on the surface of Kclay and Kaol (Ghasemi et al., 2014). The continuous increase in the adsorption amount of niobium (V) with temperature indicated that the adsorption process was endothermic. A similar result was reported that the vanadium (V) adsorption amount on montmorillonite was increased with temperature increasing (Zhu et al., 2018). With a further increase in temperature from 45 to 50 °C, the adsorption amount was slightly decreased, and the adsorption amount was 4.40 to 3.97 mg/g and 2.39 to 2.13 mg/g, respectively. The reason for the slightly declined adsorption amount from 45 to 50 °C cannot be explained well in the current work.

3.4. XRD and TEM-EDS analyses

To obtain a more comprehensive understanding of the adsorption behavior of niobium (V) on Kclay and Kaol, the variations in the characteristic diffraction reflections and the surface morphology of Kclay and Kaol before and after the adsorption with 2 mmol/L initial niobium (V) concentration were distinguished via XRD (Fig. S2, seen in Supplementary Material online) and TEM-EDS (Fig. 4). The XRD results showed that the prominent characteristic diffraction reflections of Kclay and Kaol were remarkably unchanged and there was no new diffraction reflection found during the adsorption experiments. The TEM-EDS results of Kclay and Kaol before (Fig. 4a and Fig. 4c) and after (Fig. 4b and Fig. 4d) adsorption revealed that Nb was detected on the kaolinite minerals surface in both Kclay and Kaol samples, indicating that niobium was adsorbed at the external surface or edges of kaolinite minerals.

3.5. Adsorption kinetics

The pseudo-first-order and pseudo-second-order adsorption kinetic models fitting results of niobium (V) on Kclay and Kaol are shown in Fig. 5 and Table 3. The pseudo-second-order model of niobium (V) adsorption to Kclay and Kaol fitted better than the pseudo-first-order kinetics, evidenced by the higher correlation coefficients (Table 3). This confirmed that the rate of Kclay and Kaol adsorption was likely to be controlled by chemisorption according to the pseudo-second-order adsorption kinetic model (Ho, 2006; Abidi et al., 2017). The rate constant k_2 from pseudo-second-order for niobium (V) adsorption on Kclay (0.71 $g{\cdot}mg^{-1}{\cdot}min^{-1}$) was much higher than that of Kaol (0.46 $g{\cdot}mg^{-1}{\cdot}min^{-1}$), indicating that the adsorption was more rapid at the beginning of the process for Kclay than for Kaol.

3.6. Adsorption isotherms

Adsorption isotherms models are mathematical models based on some assumptions related to the heterogeneity/homogeneity of the solid surface, the type of coverage, and the possibility of interaction between the adsorbate species (Rodrigues and da Silva, 2009; Benzaoui et al., 2018). The Langmuir and Freundlich isotherms of niobium (V)

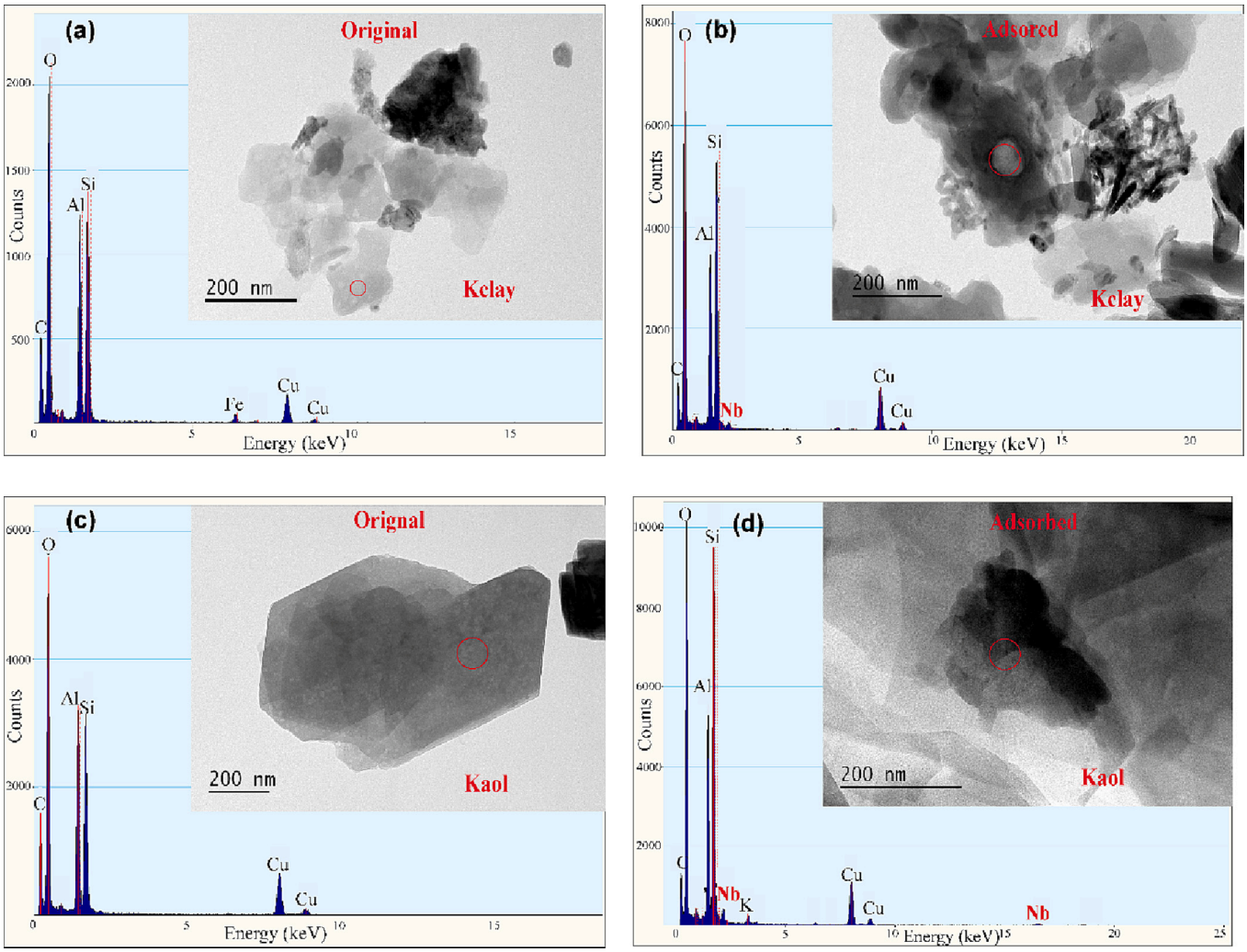

Fig. 4. TEM -EDS analysis of (a) original Kclay, (b) after niobium (V) adsorption of Kclay, (c) original Kaol, and (d) after niobium (V) adsorption of Kaol (C_0 = 2 mmol/L).

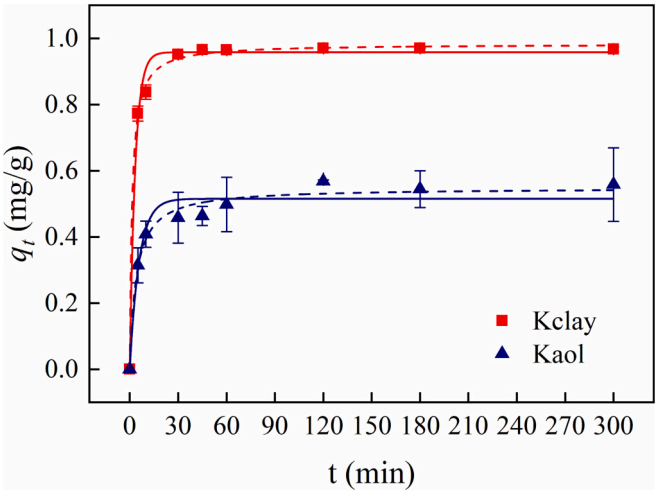

Fig. 5. Pseudo-first-order and pseudo-second-order kinetics for niobium (V) adsorption on Kclay and Kaol (S/L = 10 g/L, C_0 = 0.1 mmol/L, T = 25 °C). Symbols stand for average experimental data and the solid lines and the dash lines represent the pseudo-first-order and pseudo-second-order kinetics, respectively.

adsorption on Kclay and Kaol were obtained from Eqs. (4) and (5), as shown in Fig. 6. The Langmuir and Freundlich isotherms parameters are listed in Table 4. The data indicated that the correlation coefficients (R^2 = 0.9720) for the Freundlich equation of Kclay were slightly better than the R^2 (0.9470) for the Langmuir equation. This result agreed with the studies about chromium (VI) adsorption on kaolinite characterized by the Freundlich isotherm model (Ajouyed et al., 2011). The Langmuir isotherm model, however, fitted niobium (V) adsorption on Kaol better than the Freundlich isotherm model, indicating that the adsorption was monomolecular. The Langmuir theoretical maximum adsorption amount of Kclay and Kaol was 5.42, and 2.25 mg/g (25 °C), respectively. The value of 1/n obtained from the Freundlich isotherm was <1, which indicated that the adsorption of niobium (V) on Kclay and Kaol was a favorable process.

4. Conclusions

The niobium (V) adsorption behavior on kaolin clay (Kclay) and pure kaolinite (Kaol) was investigated in this study. The batch adsorption experiments results showed that Kclay and Kaol exhibited strong adsorption abilities on niobium (V), and the niobium (V) adsorption amount of Kclay was greater than Kaol. The adsorption of niobium (V) on Kclay reached equilibrium at 30 min with an adsorption amount of 0.97 mg/g under the conditions of 0.10 mmol/L initial niobium (V) concentration, natural pH (3.8), and 25 °C, while Kaol reached

Table 3
Kinetics parameters for niobium (V) adsorption on Kclay and Kaol.

Samples	$q_{e,\ exp}$ (mg/g)	Pseudo-first-order kinetics			Pseudo-second-order kinetics		
		k_1 (1/min)	$q_{e,\ cal}$ (mg/g)	R^2	k_2 (g·mg^{-1}·min^{-1})	$q_{e,\ ca}$ (mg/g)	R^2
Kclay	0.97	0.29	0.96	0.9917	0.71	0.98	0.9987
Kaol	0.56	0.17	0.51	0.9529	0.46	0.54	0.9815

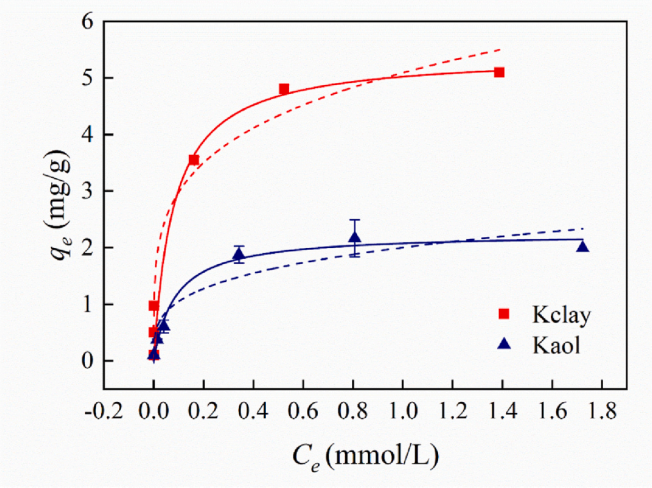

Fig. 6. Langmuir and Freundlich isotherms for niobium (V) adsorption on Kclay and Kaol (S/L = 10 g/L, T = 25 °C, t = 300 min). Symbols stand for average experimental data and the solid lines and the dash lines represent the Langmuir model and the Freundlich model, respectively.

Table 4
Isotherm parameters for niobium (V) adsorption on Kclay and Kaol.

Samples	Langmuir isotherm model			Freundlich isotherm model		
	q_{max} (mg/g)	K_L (L/mmol)	R^2	K_F [(mg/g)·(L/mmol)$^{1/n}$]	$1/n$	R^2
Kclay	5.42	12.61	0.9470	5.08	0.23	0.9720
Kaol	2.25	11.57	0.9796	2.00	0.28	0.8693

equilibrium at 120 min with an adsorption amount of 0.56 mg/g under the same conditions. The adsorptions of niobium (V) on Kclay and Kaol were pH-dependent, and they showed declining adsorption capacities from pH 2 to 4. The adsorption kinetics of niobium (V) on Kclay and Kaol fitted well with the pseudo-second-order kinetic model. The Freundlich isotherm model agreed well with the adsorption data for Kclay, while the Langmuir isotherm model suited better for the data from Kaol. The Langmuir model indicated that the maximum adsorption amount of Kclay and Kaol was 5.42 and 2.25 mg/g, respectively. The results demonstrated that niobium could be adsorbed by kaolin clay and kaolinite, providing evidence for the previous conjecture that Nb can be present in clay minerals in adsorbed form.

CRediT authorship contribution statement

Tingting Yang: Investigation, Resources, Data curation, Writing – original draft. **Ning Wang:** Conceptualization, Resources, Supervision. **Hannian Gu:** Writing – review & editing, Conceptualization, Validation, Resources, Methodology, Supervision, Funding acquisition.

Declaration of Competing Interest

The authors declare that they have no known competing financial interests or personal relationships that could have appeared to influence the work reported in this paper.

Data availability

The data that has been used is confidential.

Acknowledgments

This work was financially supported by the National Natural Science Foundation of China (41972048), Guizhou Provincial 2019 Science and Technology Subsidies (No. GZ2019SIG), the Youth Innovation Promotion Association CAS (2021400), and Guizhou Outstanding Young Scientific and Technological Talents Project (2021-5641).

Appendix A. Supplementary data

Supplementary data to this article can be found online at https://doi.org/10.1016/j.clay.2023.106866.

References

Abidi, N., Duplay, J., Jada, A., Baltenweck, R., Errais, E., Semhi, K., Trabelsi-Ayadi, M., 2017. Toward the understanding of the treatment of textile industries' effluents by clay: adsorption of anionic dye on kaolinite. Arab. J. Geosci. 10 (16), 1–14. https://doi.org/10.1007/s12517-017-3161-3.

Ajouyed, O., Hurel, C., Marmier, N., 2011. Evaluation of the adsorption of hexavalent chromium on kaolinite and illite. J. Environ. Prot. 2, 1347–1352. https://doi.org/10.4236/jep.2011.210155.

Albadarin, A.B., Collins, M.N., Naushad, M., Shirazian, S., Walker, G., Mangwandi, C., 2017. Activated lignin-chitosan extruded blends for efficient adsorption of methylene blue. Chem. Eng. J. 307, 264–272. https://doi.org/10.1007/s12517-017-3161-3.

Alshameri, A., He, H., Zhu, J., Xi, Y., Zhu, R., Ma, L., Tao, Q., 2018. Adsorption of ammonium by different natural clay minerals: characterization, kinetics and adsorption isotherms. Appl. Clay Sci. 159, 83–93. https://doi.org/10.1016/j.clay.2017.11.007.

Alshameri, A., He, H.P., Xin, C., Zhu, J.X., Xinghu, W., Zhu, R.L., Wang, H.L., 2019. Understanding the role of natural clay minerals as effective adsorbents and alternative source of rare earth elements: adsorption operative parameters. Hydrometallurgy 185, 149–161. https://doi.org/10.1016/j.hydromet.2019.02.016.

Appel, C., Ma, L.Q., Rhue, R.D., Kennelley, E., 2003. Point of zero charge determination in soils and minerals via traditional methods and detection of electroacoustic mobility. Geoderma 113, 77–93. https://doi.org/10.1016/S0016-7061(02)00316-6.

Awad, M.E., López-Galindo, A., Setti, M., El-Rahmany, M.M., Iborra, C.V., 2017. Kaolinite in pharmaceutics and biomedicine. Int. J. Pharm. 533 (1), 34–48. https://doi.org/10.1016/j.ijpharm.2017.09.056.

Benzaoui, T., Selatnia, A., Djabali, D., 2018. Adsorption of copper(II) ions from aqueous solution using bottom ash of expired drugs incineration. Adsorpt. Sci. Technol. 36 (1–2), 114–129. https://doi.org/10.1177/0263617416685099.

Brunauer, S., Emmett, P.H., Teller, E., 1938. Adsorption of gases in multimolecular layers. J. Am. Chem. Soc. 60, 309–319.

Charles, D., Prime, D., 1983. Desorption behaviour of artificial radionuclides sorbed on to estuarine silt: (I) caesium-137 and ruthenium-106, (II) zirconium-95 and niobium-95. Environ. Pollut. Ser. B. 273–295.

Dai, S., Zhou, Y., Zhang, M., Wang, X., Wang, J., Song, X., Jiang, Y., Luoa, Y., Song, Z., Yang, Z., Ren, D., 2010. A new type of Nb(Ta)-Zr(Hf)-REE-Ga polymetallic deposit in the late Permian coal-bearing strata, eastern Yunnan, southwestern China: possible economic significance and genetic implications. Int. J. Coal Geol. 83, 55–63. https://doi.org/10.1016/j.coal.2010.04.002.

Deblonde, G.J.P., Bengio, D., Beltrami, D., Bélair, S., Cote, G., Chagnes, A., 2019. Niobium and tantalum processing in oxalic-nitric media: $Nb_2O_5 \cdot nH_2O$ and $Ta_2O_5 \cdot nH_2O$ precipitation with oxalates and nitrates recycling. Sep. Purif. Technol. 226, 209–217. https://doi.org/10.1016/j.seppur.2019.05.087.

Dönmez, G., Aksu, Z., 2002. Removal of chromium(VI) from saline wastewaters by Dunaliella species. Process Biochem. 38 (5), 751–762. https://doi.org/10.1016/S0032-9592(02)00204-2.

Ervanne, H., Hakanen, M., Lehto, J., 2014. Modelling of niobium sorption on clay minerals in sodium and calcium perchlorate solutions. Radiochim. Acta 102 (9), 839–847. https://doi.org/10.1515/ract-2013-2165.
Freundlich, H.M.F., 1906. Über die adsorption in losungen. Z. Phys. Chem. 57, 385–470.
Ghasemi, M., Naushad, M., Ghasemi, N., Khosravi-Fard, Y., 2014. A novel agricultural waste based adsorbent for the removal of Pb(II) from aqueous solution: kinetics, equilibrium and thermodynamic studies. J. Ind. Eng. Chem. 20 (2), 454–461. https://doi.org/10.1016/j.jiec.2013.05.002.
Ghosh, M., Swain, K.K., Verma, R., 2017. Interaction of niobium with iron-oxide colloids and the role of humic acid. J. Environ. Radioactiv. 178, 101–109. https://doi.org/10.1016/j.jenvrad.2017.08.003.
Ghosh, M., Devi, P.R., Swain, K.K., 2019. Sorption of Nb(V) on pyrolusite(β-MnO_2): effect of pH, humic acid, ionic strength, equilibration time and temperature. Appl. Radiat. Isotopes 154, 108887. https://doi.org/10.1016/j.apradiso.2019.108887.
Ghosh, M., Yadav, A.K., Devi, P.S., Swain, K.K., Verma, R., Jha, S.N., Bhattacharyya, D., 2020. Thermodynamic and spectroscopic investigation of Nb(V) and Pa(V) sorption on colloidal silica. Environ. Earth Sci. 79 (1), 1–12. https://doi.org/10.1007/s12665-019-8781-3.
Gibson, C.E., Kelebek, S., Aghamirian, M., 2015. Niobium oxide mineral flotation: a review of relevant literature and the current state of industrial operations. Int. J. Miner. Process. 137, 82–97. https://doi.org/10.1016/j.minpro.2015.02.005.
Gu, H., Wang, N., Hargreaves, J.S.J., 2018. Sequential extraction of valuable trace elements from Bayer Process-derived waste red mud samples. J. Sustain. Metall. 4 (1), 147–154. https://doi.org/10.1007/s40831-018-0164-6.
Gulley, A.L., Nassar, N.T., Xun, S., 2018. China, the United States, and competition for resources that enable emerging technologies. Proc. Natl. Acad. Sci. U. S. A. 115 (16), 4111–4115. https://doi.org/10.1073/pnas.1717152115.
Ho, Y.S., 2006. Review of second-order models for adsorption systems. J. Hazard. Mater. 136 (3), 681–689. https://doi.org/10.1016/j.jhazmat.2005.12.043.
Ho, Y.S., McKay, G., 1999. Pseudo-second order model for sorption process. Process Biochem. 34 (5), 451–465. https://doi.org/10.1016/S0032-9592(98)00112-5.
Hu, P., Yang, H., 2013. Insight into the physicochemical aspects of kaolins with different morphologies. Appl. Clay Sci. 74, 58–65. https://doi.org/10.1016/j.clay.2012.10.003.
Jehng, J.M., Wachs, I.E., 1991. Niobium oxide solution chemistry. J. Raman Spectrosc. 22 (2), 83–89. https://doi.org/10.1002/jrs.1250220207.
Khawmee, K., Suddhiprakarn, A., Kheoruenromne, I., Bibi, I., Singh, B., 2013. Dissolution behaviour of soil kaolinites in acidic solutions. Clay Miner. 48 (3), 447–461. https://doi.org/10.1180/claymin.2013.048.3.02.
Lagergren, S., 1898. Zur theorie der sogenannten adsorption gelöster stoffe. Kungliga Svenska Vetenskapsakademiens Handlingar 24, 1–39.
Langmuir, I., 1916. The constitution and fundamental properties of solids and liquids. Part I. Solids. J. Am. Chem. Soc. 38 (11), 2221–2295. https://doi.org/10.1021/ja02268a002.
Lehto, J., Hou, X., 2010. Chemistry and Analysis of Radionuclides Laboratory Techniques and methodology. Wiley-VCH.
Mackay, D.A.R., Simandl, G.J., 2014. Geology, market and supply chain of niobium and tantalum-a review. Mineral. Deposita 49 (8), 1025–1047. https://doi.org/10.1007/s00126-014-0551-2.
MNR (Ministry of Natural Resources of the People's Republic of China), 2020. Geology Mineral Industry Standard of people's Republic of China: Specifications for Rare Metal Mineral Exploration (DZ/T 0203–2020). Geological Press, Beijing (in Chinese).
Rodrigues, L.A., da Silva, M.L.C.P., 2009. An investigation of phosphate adsorption from aqueous solution onto hydrous niobium oxide prepared by co-precipitation method. Colloids Surf. A: Physicochem. Eng. Aspects 334 (1–3), 191–196. https://doi.org/10.1016/j.colsurfa.2008.10.023.
Schlewitz, J.E., 2009. Niobium and Niobium Compounds. Kirk-Othmer Encyclopedia of Chemical Technology. Wiley, New Jersey.
Schroeder, P.A., Melear, N.D., Pruett, R.J., 2003. Quantitative analysis of anatase in Georgia kaolins using Raman spectroscopy. Appl. Clay Sci. 23 (5–6), 299–308. https://doi.org/10.1016/S0169-1317(03)00129-7.
Sei, J., Jumas, J.C., Olivier-Fourcade, J., Quiquampoix, H., Staunton, S., 2002. Role of iron oxides the phosphate adsorption properties of kaolinites from the Ivory Coast. Clay Clay Miner. 50 (2), 217–222. https://doi.org/10.1346/000986002760832810.
Sjöqvist, A.S., Cornell, D.H., Andersen, T., Erambert, M., Ek, M., Leijd, M., 2013. Three compositional varieties of rare-earth element ore: eudialyte-group minerals from the Norra Kärr Alkaline Complex, Southern Sweden. Minerals 3 (1), 94–120. https://doi.org/10.3390/min3010094.
Söderlund, M., Hakanen, M., Lehto, J., 2015. Sorption of niobium on boreal forest soil. Radiochim. Acta 103 (12), 859–869. https://doi.org/10.1515/ract-2015-2429.
Steinberg, E.P., 1961. The Radiochemistry of niobium and tantalum. In: Clear. House Fed. Sci. Tech. Inf. NAS-NS, p. 3039.
Sun, L., Zhang, X., Wang, L., Yu, H., Meng, F., Qi, T., Peng, Y., 2022. Separation and extraction of niobium from H_2SO_4 solution containing titanium and iron impurities. Sep. Purifi. Technol. 121207 https://doi.org/10.1016/j.seppur.2022.121207.
Tombácz, E., Szekeres, M., 2006. Surface charge heterogeneity of kaolinite in aqueous suspension in comparison with montmorillonite. Appl. Clay Sci. 34, 105–124. https://doi.org/10.1016/j.clay.2006.05.009.
USGS, 2022. Mineral commodity summaries. Niobium (Columbium) 116–117. https://doi.org/10.3133/mcs2022.
Wang, N., Gu, H., Wen, H., Liu, S., 2018. Enrichment of niobium and titanium from kaolin using an acid-alkali leaching process. Metall. Mater. Trans. B Process Metall. Mater. Process. Sci. 49 (6), 3552–3558. https://doi.org/10.1007/s11663-018-1405-6.
Yamaguchi, T., Ohira, S., Hemmi, K., Barr, L., Shimada, A., Maeda, T., Iida, Y., 2020. Consideration on modeling of Nb sorption onto clay minerals. Radiochim. Acta 108 (11), 873–877. https://doi.org/10.1515/ract-2020-0006.
Yu, W., Xu, H., Tan, D., Fang, Y., Roden, E.E., Wan, Q., 2020. Adsorption of iodate on nanosized tubular halloysite. Appl. Clay Sci. 184, 105407 https://doi.org/10.1016/j.clay.2019.105407.
Zhang, Z., Zheng, G., Takahashi, Y., Wu, C., Zheng, C., Yao, J., Xiao, C., 2016. Extreme enrichment of rare earth elements in hard clay rocks and its potential as a resource. Ore Geol. Rev. 72, 191–212. https://doi.org/10.1016/j.oregeorev.2015.07.018.
Zhao, L., Dai, S., Graham, I.T., Li, X., Zhang, B., 2016a. New insights into the lowest Xuanwei Formation in eastern Yunnan Province, SW China: implications for Emeishan large igneous province felsic tuff deposition and the cause of the end-Guadalupian mass extinction. Lithos 26, 375–391. https://doi.org/10.1016/j.lithos.2016.08.037.
Zhao, L., Dai, S., Graham, I.T., Wang, P., 2016b. Clay mineralogy of coal-hosted Nb-Zr-REE-Ga mineralized beds from Late Permian strata, eastern Yunnan, SW China: implications for paleotemperature and origin of the micro-quartz. Minerals 6 (45), 1–17. https://doi.org/10.3390/min6020045.
Zhao, L., Dai, S., Graham, I.T., Li, X., Liu, H., Song, X., Hower, J.C., Zhou, Y., 2017. Cryptic sediment-hosted critical element mineralization from eastern Yunnan Province, southwestern China: mineralogy, geochemistry, relationship to Emeishan alkaline magmatism and possible origin. Ore Geol. Rev. 80, 116–140. https://doi.org/10.1016/j.oregeorev.2016.06.014.
Zhu, H., Xiao, X., Guo, Z., Han, X., Liang, Y., Zhang, Y., Zhou, C., 2018. Adsorption of vanadium (V) on natural kaolinite and montmorillonite: characteristics and mechanism. Appl. Clay Sci. 161, 310–316. https://doi.org/10.1016/j.clay.2018.04.035.
Zhu, L., Gu, H., Yang, Y., Wen, H., Du, S., Luo, C., Wang, N., 2021. Occurrence modes of niobium in kaolin clay from Guizhou, China. Mining Metall. Explor. 38 (2), 855–862. https://doi.org/10.1007/s42461-020-00363-x.